

### Centrifuge method mix compositions

All compositions of the cement paste had the same initial solids volume fraction of 0.45, which corresponds to a water-binder ratio ( $w/b$ ) of about 0.41 for the control mix. The mix compositions were derived from the SFSCC mixes. As such, 30% of the portland cement was replaced by fly ash, by mass. Also, a naphthalene-based HRWR was used. In this particular study, clay dosages for C1 were varied in order to find an optimal amount. The mix compositions are given in Table 6.

**Table 6—Compressive rheology mix composition**

Mix identifier	Cement, g (lb)	Fly ash, g (lb)	Water, g (lb)	HRWR, g (lb)	C1, g (lb)
A1	891 (1.96)	382 (0.842)	545 (0.120)	6.37 (0.0140)	0
A2	887 (1.96)	380 (0.838)	545 (0.120)	6.33 (0.0140)	6.33 (0.0140)
A3	882 (1.94)	378 (0.833)	545 (0.120)	6.30 (0.0139)	12.6 (0.0278)
A4	877 (1.93)	376 (0.829)	545 (0.120)	6.27 (0.0138)	18.8 (0.0414)

In addition to the centrifuge tests, green strength tests as discussed previously were also performed on concretes made from the same paste proportions to compare to the compressive rheology results. For the green strength tests, a coarse aggregate to fine material ratio of 1.75 and a fine aggregate to fine material ratio of 1.56 were used for all concrete mixes. The coarse aggregate consisted of a round pea gravel with a maximum size of 10 mm (0.39 in) while the fine aggregate consisted of a river sand with a maximum size of 4.75 mm (0.19 in) and a fineness modulus of 2.58.

### Compressive rheology and green strength results

The compressive yield stress is plotted against the sediment volume fraction for different addition rates (0.5, 1.0 and 1.5% by mass of binder) for C1 in Fig. 12. C1 increases  $\sigma_y$  over the range of  $\phi$  shown. Figure 12 also shows the optimal dosage as 1.0% for C1. Any additional clay decreases the  $\sigma_y$  curve. The reasons for this optimum are still under research. Possible reasons include chemical changes to the suspension, changes in water content due to absorption and changes to the particle packing of the system. These results demonstrate how small additions can have large effects on the  $\sigma_y$ , similar to what has been seen in SF-SCC previous work<sup>22, 23, 28</sup>. Green strength results are shown in Fig. 13. Similar to the compressive yield stress results, C1 improves the green strength. The optimal dosage is again seen for 1.0% by mass of cement. This investigation has shown a direct relationship between macro and micro behaviors which suggests the influence of flocculation strength on green strength.

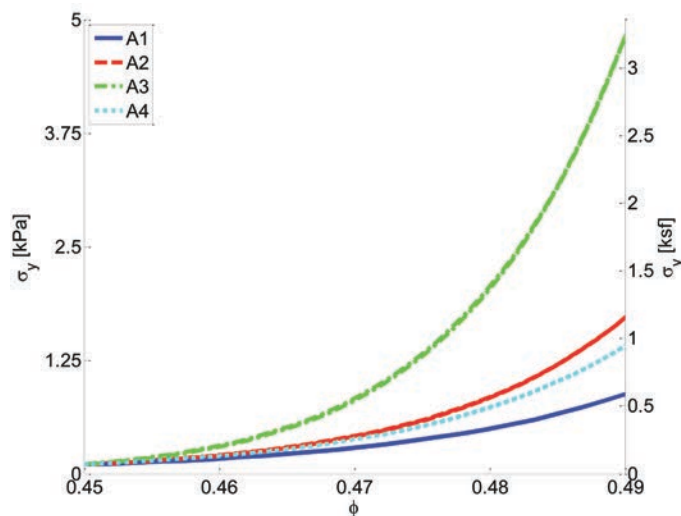


Fig. 12—Centrifuge results for C1.

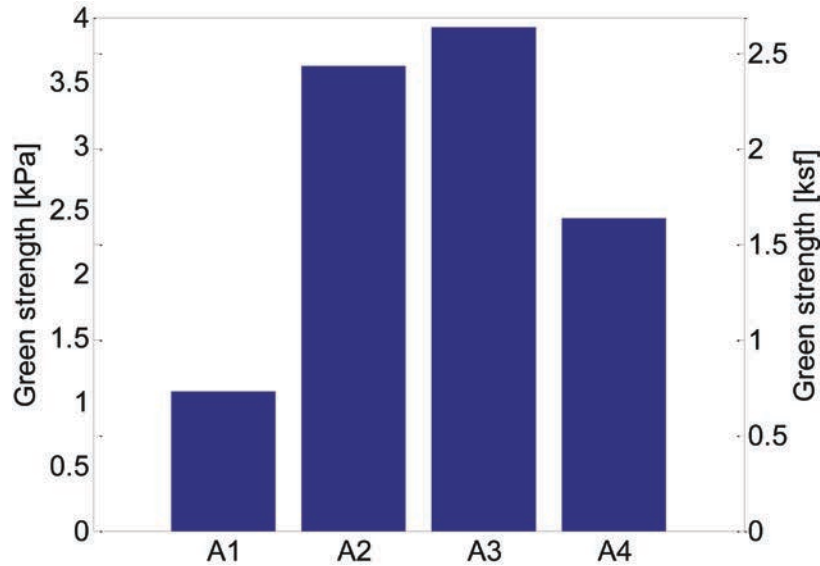


Fig. 13—Green strength results for C1.

**Focus beam reflective measurement method and mix compositions**

A novel experimental method using a focused beam reflectance measurement (FBRM) probe was recently used to examine the floc size evolution of concentrated cement paste suspensions subjected to shear stresses<sup>29</sup>. The FBRM method is a particle size analysis measurement technique that provides information about particle chord length distribution in real-time. The significant advantage of the FBRM method is that no dilution or sampling of the suspension is required which is especially important for cement pastes. FBRM instruments operate by scanning a highly focused laser beam across particles in a suspension and measuring the time duration of back scattered light from individual particles<sup>30,31</sup>.

This is one of the first experiments for in-situ investigations of the microstructural response of concentrated cement paste suspensions subjected to shear-induced stresses. The FBRM floc size measurements were conducted while subjecting the sample to a 40 rpm mixing intensity followed by a 400 rpm mixing intensity. Generally, higher count numbers indicate mixtures with fresh state microstructures that have a lower degree of flocculation.

A Type I portland cement with a relatively high equivalent alkali content (0.85%) was used in addition to a polycarboxylate-based HRWR and C3. The mix compositions are shown in Table 7.

**Table 7—FBRM mix composition**

Mix identifier	w/b	HRWR, % binder	C3, % replacement of binder
A1	0.40	0.14	0
A2	0.40	0.14	1.5

**FBRM results**

In Fig. 14, the evolution of the mean chord size is compared between a cement paste (A1) and a cement paste containing C3 (A2). The results show that with only 1.5% of the cement replaced by C3, there is an increase in the mean chord size at both high and low shear. This indicates that strength between the flocs is higher for A2 compared to A1. In addition, during the low shear, A2 increases in size at a faster rate (note the higher slope between 50 and 70 minutes for A2).

In Fig. 15, the distribution of chord lengths is presented as a difference in distributions between the start of a rest period and the end. As a general trend for both mixes, during low shear, the number of smaller particles decreases while the number of larger particles increases. This indicates that smaller flocs are combining to form larger ones. For A2, this process is more dramatic, indicating a higher degree of flocculation.

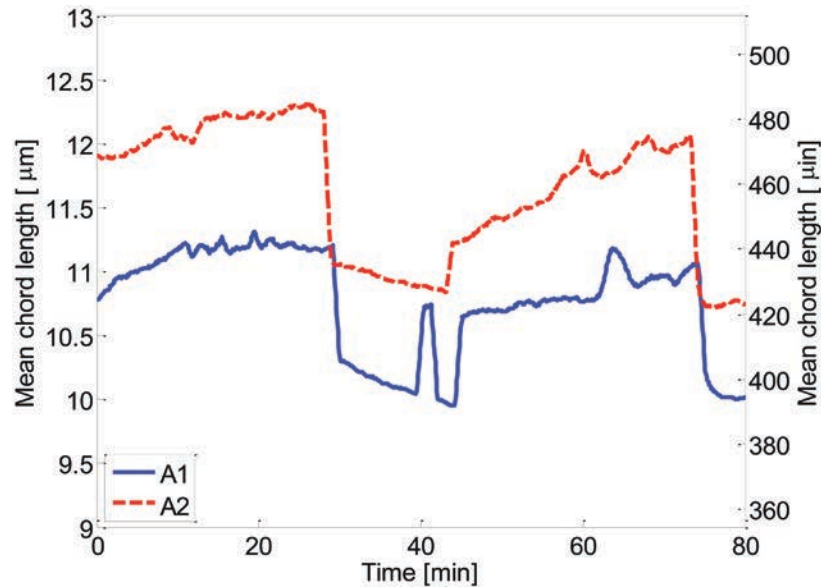


Fig. 14—Evolution of mean chord length between Mixtures A1 and A2.

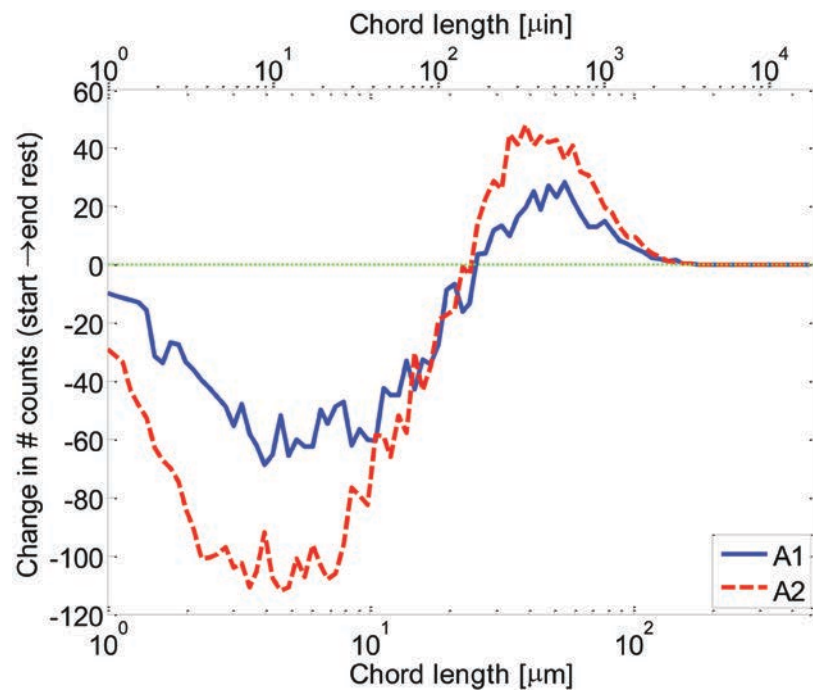


Fig. 15—Difference in counts between start and end of rest period for Mixtures A1 and A2.

## CONCLUSIONS

This summary paper of ACBM's recent work has demonstrated the effectiveness of small additions such as metakaolinite and magnesium aluminosilicate clays on fresh-state properties of cement-based materials. Clays were found to improve shape stability in extrusion and slipform applications. In addition, clays were shown to increase the rate of stiffening and as a result, reduce lateral formwork pressure. ACBM has also looked into different methods to characterize the microstructural changes that occur with additions of clays. A centrifuge method demonstrated that clays increase the compressive yield stress, which is an indicator of flocculation strength, while an FBRM method showed that clays increase

the size of the flocs, which is an indicator of the degree of flocculation. Future work will focus on ways to optimize the use of clays as well as further characterization of microstructural changes.

## ACKNOWLEDGEMENTS

The first author would like to acknowledge financial support from both the Infrastructure Technology Institute at Northwestern University and the Center for Portland Cement Concrete Pavement Technology at Iowa State University. The second author would like to acknowledge financial support from an NSF PATH Grant No. CMS-0122045, while the third and fourth authors would like to acknowledge financial support from an NSF Award No. CMS-0625606 and support from the Infrastructure Technology Institute at Northwestern University. The fifth author would like to acknowledge an NSF award No. CMS-0625606, and financial support from the Strategic Development Council of ACI and the Ready-Mix Concrete Research Foundation. FBRM experiments were conducted in the laboratories of Dr. Carlos Negro at the Complutense Universidad in Madrid, Spain.

## REFERENCES

1. Siddique, R., and Klaus, J., "Influence of Metakaolin on the Properties of Mortar and Concrete: A Review," *Applied Clay Science*, V. 43, No. 3-4, 2009, pp. 392-400.
2. Badogiannis, E.; Papadakis, V.; Chaniotakis, E.; and Tsvilis, S., "Exploitation of Poor Greek Kaolins: Strength Development of Metakaolin Concrete and Evaluation by Means of k-Value," *Cement and Concrete Research*, V. 34, No. 6, 2004, pp. 1035-1041.
3. Poon, C.; Lam, L.; Wong, Y.; and Wong, R., "Rate of Pozzolanic Reaction of Metakaolin in High-Performance Cement Pastes," *Cement and Concrete Research*, V. 31, No. 9, 2001, pp. 1301-1306.
4. Wild, S.; Khatib, J.; and Jones, A., "Relative Strength, Pozzolanic Activity and Cement Hydration in Superplasticised Metakaolin Concrete," *Cement and Concrete Research*, V. 26, No. 10, 1996, pp. 1537-1544.
5. Bredy, P.; Chabannet, M.; and Pera, J., "Microstructural and Porosity of Metakaolin Blended Cements," *Materials Research Society Symposium*, V. 137, 1989, pp. 431-436.
6. Active Minerals Company LLC, "What is Acti-Gel® 208 and How is it Made?" 2007.
7. Stephan Schmidte Gruppe, "Technisches Datenblatt Coneresol® 105," 2004. (in German)
8. Engelhard, "MetaMax High-Reactivity Metakolin for Concrete," 2008, [http://www2.basf.us/functional\\_polymers/kaolin/pdfs/TechnicalDataSheet.pdf](http://www2.basf.us/functional_polymers/kaolin/pdfs/TechnicalDataSheet.pdf).
9. Peled, A.; Cyr, M.; and Shah, S., "High Content of Fly Ash (Class F) in Extruded Cementitious Composites," *ACI Materials Journal*, V. 97, No. 5, Sept.-Oct. 2000, pp. 509-517.
10. Burke, P., and Shah, S., "Durability of Extruded Thin Sheet PVA Fiber-Reinforced Cement Composites," *High-Performance Fiber-Reinforced Concrete Thin Sheet Products*, SP-190, American Concrete Institute, Farmington Hills, MI, 2000, pp. 133-164.
11. Kuder, K., and Shah, S., "Rheology of Extruded Cement-Based Composites," *ACI Materials Journal*, V. 104, No. 3, May-June 2007, pp. 283-290.
12. Bagley, E., "End Correction in the Capillary Flow of Polyethylene," *Journal of Applied Physics*, V. 28, 1957, pp. 624-627.
13. ACI Committee 347, "Guide to Formwork for Concrete (ACI 347-04)," American Concrete Institute, Farmington Hills, MI, 2005, 32 pp.
14. Billberg, P.; Silwerbrand, J.; and Osterberg, T., "Form Pressures Generated by Self-Consolidating Concrete," *Concrete International*, V. 27, No. 10, Oct. 2005, pp. 35-42.
15. Tejada-Dominguez, F.; Lange, D.; and D'Ambrosia, M., "Formwork Pressure of Self-Consolidating Concrete in Tall Wall Field Applications," *Journal of the Transportation Research Board*, V. 1914, 2005, pp. 1-7.
16. Khayat, K., and Assaad, J., "Effect of  $w/cm$  and High-Range Water-Reducing Admixture on Formwork Pressure and Thixotropy of Self-Consolidating Concrete," *ACI Materials Journal*, V. 103, No. 3, May-June 2006, pp. 186-193.
17. Gregori, A.; Ferron, R.; Sun, Z.; and Shah, S., "Experimental Simulation of Self-Consolidating Concrete Formwork Pressure," *ACI Materials Journal*, V. 105, No. 1, Jan.-Feb. 2008, pp. 97-104.
18. Assaad, J., and Khayat, K., "Effect of Viscosity-Enhancing Admixtures on Formwork Pressure and Thixotropy of Self-Consolidating Concrete," *ACI Materials Journal*, V. 103, No. 4, July-Aug. 2006, pp. 280-287.
19. Assaad, J., and Khayat, K., "Effect of Coarse Aggregate Characteristics on Lateral Pressure Exerted by Self-Consolidating Concrete," *ACI Materials Journal*, V. 102, No. 3, May-June 2006, pp. 145-153.
20. Kwon, S.; Shah, S.; Phung, Q.; Kim, J.; and Lee, Y., "Experimental Simulation of Self-Consolidating Concrete Formwork Pressure," *ACI Materials Journal*, V. 107, No. 1, Jan.-Feb. 2010, pp. 20-30.
21. Ardani, A.; Hussain, S.; and LaForce, R., "Evaluation of Premature pcc Pavement Longitudinal Cracking in Colorado," *Proceedings of the 2003 Mid-Continent Transportation Research Symposium*, Iowa State University,

## 66 Tregger et al.

- Ames, IA, 2003.
22. Pekmezci, B.; Voigt, T.; Wang, K.; and Shah, S., "Low Compaction Energy Concrete for Improved Slipform Casting of Concrete Pavements," *ACI Materials Journal*, V. 104, No. 3, May-June 2007, pp. 251-258.
  23. Tregger, N.; Voigt, T.; and Shah, S., "Improving the Slipform Process Via Material Manipulation," *Advances in Construction Materials*, C. Grosse, ed., Springer Berlin Heidelberg, 2007.
  24. European Standard EN 206, "Concrete Part 1: Specification, Performance, Production and Conformity," British Standards Institute, 2001.
  25. Wyss, H.; Tervoort, E.; and Gauckler, L., "Mechanics and Microstructures of Concentrated Particle Gels," *Journal of the American Ceramics Society*, V. 88, No. 9, 2005, pp. 2337-2348.
  26. Buscall, R., and White, L., "On the Consolidation of Concentrated Suspensions I: The Theory of Sedimentation," *Journal of Chemical Societies Faraday Transactions*, V. 83, No. 3, 1987, pp. 873-891.
  27. Green, M.; Eberl, M.; and Landman, K., "Compressive Yield Stress of Flocculated Suspensions: Determination Via Experiment," *American Institute of Chemical Engineering Journal*, V. 42, No. 8, 1996, pp. 2308-2318.
  28. Tregger, N.; Knai, H.; and Shah, S., "Flocculation Behavior of Cement Pastes Containing Clays and Fly Ash," *Transition from Fluid to Solid: Re-Examining the Behavior of Concrete at Early Ages*, SP-259, K. Riding, ed., American Concrete Institute, Farmington Hills, MI, 2008, 240 pp.
  29. Ferron, R., "Formwork Pressure of Self-Consolidating Concrete: Influence of Flocculation Mechanisms, Structural Rebuilding, Thixotropy and Rheology," PhD dissertation, Department of Civil and Environmental Engineering, Northwestern University, Evanston, IL, 2008.
  30. Blanco, A.; Fuente, E.; Negro, C.; and Tijero, J., "Flocculation Monitoring: Focused Beam Reflectance Measurement as a Measurement Tool," *Canadian Journal of Chemical Engineering*, V. 80, 2002, pp. 734-740.
  31. Blanco, A.; Negro, C.; Fuente, E.; and Tijero, J., "Effect of Shearing Forces and Flocculant Overdose on Filler Flocculation Mechanisms and Floc Properties," *Industrial and Engineering Chemistry Research*, V. 44, 2005, pp. 9105-9112.

# **Cement-Based Materials Characterization at Nanoscale: Nanoindentation and Ultrasonic Atomic Force Microscopy (AFM)**

**by J. H. Kim, P. Mondal, and S. P. Shah**

**Synopsis:** Characterizing mechanical properties of cement-based materials is a basic task to be performed before using it as a structural material. An array of different mechanical tests has been developed and applied to measure the stiffness or strength of materials. A recent addition to this field concerns nano-mechanical characterization. It is an extension of our interests: how rigid is a certain volume of materials in nanoscale space? Measuring the properties of interfacial transition zone (ITZ) locating between an inert aggregate and bulk paste is a key application example for nanoscale characterization. In order to measure the properties of ITZ, spatial resolution should be enhanced less than the size of ITZ (a few tens of micrometers), while the compressive strength test, a conventional macroscale measurement, usually uses a specimen of 150 mm diameter 300 mm height (6 in by 12 in) cylinder. This paper discusses two nanoscale techniques, that is, nanoindentation and ultrasonic atomic force microscopy (AFM) used at the center for Advanced Cement-Based Materials (ACBM). The principle of both techniques measuring the elastic modulus at the nanoscale is clarified with an application to a cement paste sample having 50% water-binder ratio. The measurements by both techniques are not exactly the same due to their different mechanism. However, both techniques identically find that the peak probability of the measured elastic modulus of the cement paste is distributed between 10 and 20 GPa (1450 and 2900 ksi).

**Keywords:** atomic force microscopy (AFM); cement paste; contact stiffness; elastic modulus; nanomechanics; scanning probe microscopy (SPM); spatial resolution.

**Jae Hong Kim** is a Postdoctoral Fellow at the Center for Advanced Cement-Based Materials (ACBM), Northwestern University, Evanston, IL. He received his BS, MS, and PhD from the Korea Advanced Institute of Science and Technology (KAIST) in 2002, 2004, and 2008, respectively. His research interests include the nanomechanics of cement-based materials, self-consolidating concrete, nondestructive testing, and nonlinear analysis of concrete structures.

**Paramita Mondal** is an Assistant Professor of civil and environmental engineering at the University of Illinois at Urbana-Champaign, Urbana, IL. She received her BS from Jadavpur University, India, in 2001; her MS from the University of Connecticut, Storrs, CT, in 2004; and her PhD from Northwestern University in 2008. Her research interests include nano- and micro-scale characterization of cementitious materials, nano- to macro-scale modeling, and the use of nanotechnology to improve properties and performance of concrete.

**Surendra P. Shah**, FACI, is the Walter P. Murphy Professor of Civil and Environmental Engineering and the Director of the Center for Advanced Cement-Based Materials at Northwestern University. He received the ACI Arthur R. Anderson Award in 1989 and the Robert Philleo Award in 2006 and was inducted into the National Academy of Engineering in 2006. His research interests include constitutive relationships, nondestructive testing, failure and fracture of concrete, durability, fiber-reinforced concrete, and self-consolidating concrete.

## INTRODUCTION

Concrete is an inherently heterogeneous material produced by mixing water, cement, and aggregates. Even though structural concrete can be assumed to show homogeneous behavior at the macroscale, e.g. the ACI 318 viewpoint of materials, it is important to investigate its heterogeneity composing the effective material properties to gain a better understanding of the material. The heterogeneity of cement-based materials is found immediately at different length scale. For example, at the microscale, hardened mortar has three phases: sand, cement paste, and interfacial transition zone (ITZ). Cement paste is also composed of various types of hydration products such as calcium silicate hydrate (C-S-H) and calcium hydroxide (CH). A microscale technique for materials characterization is required considering typical dimensions of those components: 20-40  $\mu\text{m}$  thick ITZ [788-1576  $\mu\text{in}$ ], 0.1-1  $\mu\text{m}$  spine C-S-H [3.94-39.4  $\mu\text{in}$ ], and 10-100  $\mu\text{m}$ -crystal CH [394-3940  $\mu\text{in}$ ].

Various investigations to understand the micro-structure of cement-based materials have been accomplished by studying its surface structure<sup>2-5</sup>. Scanning electron microscopy (SEM) and atomic force microscopy (AFM) are excellent methods to characterize the surface morphology. However, measuring local mechanical properties at the nanoscale requires a probe-based method. This paper reviews two techniques to measure the nano-mechanical properties of cement-based materials, as studied at the center for Advanced Cement-Based Materials (ACBM): nanoindentation and ultrasonic AFM.

Nanoindentation is one of the most-widely adopted techniques for this purpose of nanoscale characterization and determines an elastic modulus based on the measured indenting force-displacement curve. The slope of the curve yields the contact stiffness of the materials. Among various methods to calculate the hardness and modulus from the curve, Oliver and Pharr's method has been widely adopted because of its reliable/concise hypothesis<sup>6,7</sup>. In the field of material science of concrete, nanoindentation has become a powerful tool for nanoscale characterization<sup>8-15</sup>.

Ultrasonic AFM, otherwise known as atomic force acoustic microscopy (AFAM), is a different type of technique that measures the contact stiffness of a material based on information from a vibrating tip making contact with a sample. AFM is a scanning probe microscopy (SPM) method used to investigate the surface structure of a sample. For example, contact-mode AFM obtains topographic image of a sample surface by controlling the tip-sample distance while maintaining a constant atomic force between the cantilever tip of an AFM probe and the sample surface. This principle can be also applied to characterize the nano-mechanical properties. Force modulation microscopy (FMM) measures the resultant load experienced by the probe while applying lateral displacement onto a sample and determines the storage and loss modulus of a sample surface<sup>16,17</sup>. Ultrasonic force microscopy (UFM) uses the nonlinearity of the atomic force and evaluates the sample stiffness based on the vibration amplitude threshold to invoke the cantilever lift-off<sup>18-20</sup>. Lastly, AFAM employs the resonant frequency of the cantilever in contact

with a sample, where the contact-resonant frequency depends on the sample stiffness<sup>21-24</sup>. These methods are called ultrasonic AFM<sup>25</sup> or acoustic SPM<sup>26</sup>.

Details of both techniques are discussed in the following section, conveying their basic assumptions. In addition, their application results to cement paste, as an example, are also presented. The results here are a summary of the previous studies<sup>15,27</sup>.

## RESEARCH SIGNIFICANCE

Materials characterization at the nanoscale is an upcoming issue in the field of science and engineering. Due to the heterogeneity of cement-based materials, the nanoscale characterization of mechanical properties is significant for understanding their basic micro-structures. The research presented in this paper provides fundamental ideas of two nanoscale techniques to realize their measurements in nature. Their applications to cement paste material characterization are presented to ensure the relevancy.

## TECHNIQUES

### Nanoindentation

Nanoindentation directly measures the mechanical response of materials to a locally-applied force via a probe. The probe applies an external force to a sample, so the reliability of nanoindentation depends on the probe tip and its contact with the sample. A Berkovich tip having a shape of a geometrically self-similar triangular pyramid is generally used for the Oliver and Pharr's method<sup>6</sup>. The tip has a 142.3 degree included angle and its contact geometry is illustrated in Fig. 1(a).

An indenting force causes elastoplastic deformation locally, and then the conservative force of the sample equilibrates to the external force. Elastoplastic deformation mainly occurs at the first loading and leaves an indenter mark behind. In the unloading step, plastic deformation is minimized and the elastic resistance prevails. This phenomenon is shown in Fig. 2, an example of measured indenting force-displacement curves, where multiple loading-and-unloading steps were performed. The example curve clarifies elastic resistance governing the material behavior after the first loading. Finally, the slope of the unloading part determines the contact stiffness  $k^*$  of the probe tip and sample:

$$k^* = \frac{dP}{dh} \quad (1)$$

where  $P$  and  $h$  are the indenting force and displacement relative to the initial undeformed surface, respectively. The original Oliver and Pharr method<sup>6,7</sup> provides a reliable procedure to determine the indentation modulus with the measured contact stiffness.

### Ultrasonic AFM

Ultrasonic AFM approaches the problem in a different way: determine the resonant frequency of an AFM probe cantilever making a contact with a sample<sup>21</sup>. The resonant frequency of the probe cantilever depends on the contact stiffness composed of the probe tip and sample. For instance, hard materials increase the contact stiffness and results in a high resonant frequency. The probe cantilever can be idealized as a clamped-free spring-coupled beam, as shown in Fig. 3(b), and analyzed by the Bernoulli-Euler beam theory<sup>28</sup>. The characteristic equation for the clamped-free spring-coupled boundary derives a relationship between the contact stiffness and the contact eigenvalue (related to the resonant frequency).

The contact stiffness is determined using the Bernoulli-Euler beam theory with measured contact-resonant frequency. The resonant frequency is expressed as a function of an eigenvalue  $\lambda$  according to the theory:  $(2\omega fr)^2 = (EI/\rho A) \cdot \lambda^2$ , where  $E$ ,  $I$ ,  $\rho$ ,  $A$  are the Young's modulus, the second moment of inertia, the mass density and the cross-sectional area of the probe cantilever, respectively. Each value of the cantilever properties is hard to be obtained separately, so the value of  $(EI/\rho A)$  is determined with the known eigenvalue and by measuring the resonant frequency of a free cantilever before making a contact. Once the probe cantilever makes contact with the sample surface, the contact stiffness ( $k^*$ ) is realized and the characteristic equation determining the contact-eigenvalue  $\lambda^*$  is derived<sup>21</sup>:

$$\frac{k^*}{k} = \frac{1}{3} (\lambda^* L)^3 \frac{1 + \cosh \lambda^* L \cos \lambda^* L}{\sinh \lambda^* L \cos \lambda^* L - \cosh \lambda^* L \sin \lambda^* L} \quad (2)$$

where  $k$  is the stiffness of the probe cantilever:  $k=3EI/L^3$  with the cantilever length of  $L$ . Eq. (2) is one of the relationships between the measured contact-resonant frequency and the estimated contact stiffness.

In summary, a typical procedure for ultrasonic AFM is as follows. (1) Measure the resonant frequency ( $f_r$ ) of the probe cantilever without making contact, i.e. free vibration. This is to evaluate the cantilever property required for establishing the relationship between the resonant frequency and eigenvalue. (2) Measure the contact-resonant frequency ( $f_r^*$ ) once a static load is applied and contact with the sample surface is realized. The corresponding contact-eigenvalue can be calculated with the evaluated cantilever property beforehand. (3) Calculate the contact stiffness using the above relationship. In actual experiments, the probe cantilever has a branch out of the probe tip, so a more sophisticated relationship instead of Eq. (2) was used for considering a branch-out length<sup>22</sup>.

### Comprehension and comments

The first-hand result of both techniques is the contact stiffness ( $k^*$ ) implying the elastic resistance of the probe tip graft on the sample. Assuming that the sample is isotropic homogeneous and its surface is flat and frictionless at the nanoscale, a contact theory<sup>29</sup> can determine the reduced modulus ( $E^*$ ), defined as Eq. (3), from the contact stiffness.

$$\frac{1}{E^*} = \frac{1-\nu_{tip}^2}{E_{tip}} + \frac{1-\nu^2}{E} \quad (3)$$

where  $E$  and  $\nu$  are the Young's modulus and Poisson's ratio of the sample, respectively. Those of the probe tip are denoted as  $E_{tip}$  and  $\nu_{tip}$ , respectively. Both techniques adopt the same contact theory to analyze their measurements, but the only difference is on the shape of the probe tip. Ultrasonic AFM uses a general AFM probe and its tip is considered spherical (Hertzian contact), while the Berkovich tip used for nanoindentation has a triangular lateral-section, as shown in Fig. 1(a) and Fig. 3(a). Therefore, the contact theory relating the measured variable to the final result is one of the important issues ensuring the accuracy of the techniques.

In addition to the difference in the shape of the contacts in these two methods, the size of contacts should be accounted for. Ultrasonic AFM produces a comparatively small size of the contact, generally about 20 nm (0.788  $\mu\text{m}$ ) diameter, which is identical to that for a contact-mode AFM. However, the Berkovich tip has about 1  $\mu\text{m}$  (39.4  $\mu\text{m}$ ) diameter contact (indent) area providing the large amount of indenting force. The indenting force could be as high as 1 mN ( $225 \times 10^{-6}$  lb), but the static load for the AFM probe is less than 1  $\mu\text{N}$  ( $0.225 \times 10^{-6}$  lb). The spatial resolution of the techniques is governed by the contact area, and ultrasonic AFM has the merit of a more delicate-localized measurement. In the case of our examples, ultrasonic AFM is promising for modulus-gradation measurements within the 20-40  $\mu\text{m}$  (788-1576  $\mu\text{m}$ ) thick ITZ.

In spite of the high-quality spatial resolution of ultrasonic AFM, it is still hard to measure the properties of a solid C-S-H particle excluding the effect of pores. That is deduced from the fact that capillary and gel pores in amorphous C-S-H are randomly distributed with the size of 1 nm to 50 nm (0.0394  $\mu\text{m}$  to 1970  $\mu\text{m}$ ). Therefore, nanoindentation, which gives the effective modulus with respect to the indenter area, would be more attractive for homogenization of nano-properties related to multi-scale modeling<sup>12,13,30,31</sup>.

Inherent mechanisms for both techniques give a chance to consider an interesting comparison between the nanoscale techniques and macroscale measurements. Nanoindentation and ultrasonic AFM can be compared with the static modulus by compression testing (ASTM C469)<sup>32</sup> and the dynamic modulus by resonant frequency method (ASTM C215)<sup>33</sup>, respectively. Nanoindentation uses slow loading rates and the large amount of indenting force resulting in plastic deformation. This is similar to ASTM C469 resulting in inelastic deformation of a specimen. However, the static force to make contact for ultrasonic AFM is extremely less than the indenting force and results in inducing no plastic deformation, and ultrasonic AFM measures the resonant frequency at the level of applied strain. Even though ultrasonic AFM measures the resonant frequency of the probe cantilever graft on the sample, different from ASTM C215 measuring that of the sample, the contact stiffness affecting the measured resonant frequency corresponds to the dynamic modulus inducing very small strain within elastic deformation.

## APPLICATIONS

### Sample preparation

Both techniques were performed on a cement paste sample. The sample of 25 mm × 25 mm × 25 mm (1 in × 1 in × 1 in) was made out of Type I portland cement with a water-to-cement ratio of 0.5 by weight. It was demolded after 1 day, and then cured at 25°C (77°F) under water for 2 years. Once cured, an approximate 5 mm (0.25 in) thick piece was cut out of the cube and mounted on a metal sample for polishing its surface. Having a smooth flat surface is necessary for reliable measurement. The polishing was started with a 320 grit, then 600, followed by 1200 grid size, and finally diamond lapping films of gradation 6 μm and 3 μm (236 μin and 118 μin). It was finished with a diamond suspension in water of 0.1 μm (3.94 μin) on a polishing cloth. Details can be found elsewhere.<sup>15</sup>

### Details and results

Nanoindentation was performed with an automated nano-mechanical test system. The indenter having the Berkovich tip was positioned within the surface area of 60 μm × 60 μm (2360 μin × 2360 μin). Multiple cycles of partial loading and unloading were used to make each indent, eliminating the effect of plastic deformation. Figure 2 shows the measured indenting-force and displacement. The contact stiffness becomes the slope of the unloading part and the Oliver and Pharr method was used to determine the indentation modulus dividing the maximum indentation load by the contact area. A total of 36 measurements on hydrates were accomplished.

Ultrasonic AFM requires special devices in addition to a conventional AFM instrument. The study adopts a forced-vibration system for acoustic modification. A waveform generator to create frequencies of up to 20 MHz; and a rock-in amplifier to analyze 25 kHz to 200 MHz signals with 16-bit digital-to-analogue and analogue-to-digital converters were assembled. The cantilever behavior was measured with a photo-detector attached to an AFM instrument. The rock-in signals of the cantilever behavior were recorded to build the resonant spectrum using a data acquisition device, where the device has a maximum sampling rate of 1.25 MS/s and 16 bits resolution. Thirty-four locations within the 5 mm × 5 mm (0.2 in × 0.2 in) region of the surface were randomly selected and the contact-resonant spectrums were measured. The indentation modulus for each location was calculated based on the measured contact-resonant frequency.

The measurements at randomly selected locations on the sample could be considered as a random process to represent the distribution of the measured elastic modulus. The indentation moduli  $M=E/(1-\nu^2)$  obtained by each technique are not exactly the same, as shown in Fig. 6. This discrepancy could be explained with the mechanism of the measurements and the micro-structure of cement paste. It is thought that the plastic deformation of nanoindentation is mainly due to capillary/gel pores destruction by the indentation. The pore destruction results in an indent mark on the sample surface, and also the cement paste is finally consolidated. The consolidation of cement paste could explain that the mean modulus measured by nanoindentation is 20.5 GPa (2973 ksi) greater than 14.7 GPa (2132 ksi) done by ultrasonic UFM. In addition to pore destruction, the spatial resolution described already affects the results of measurement. Various particles such as two types of C-S-H and CH can be placed under 1 μm (39.4 μin) diameter contact (indent) area of nanoindentation, and then its measurement is thought to be an effective modulus corresponding to the indent area. It was reported that its results is reliable to evaluate the properties of each nano-particle via an inverse analysis<sup>12,13</sup>. On the other hand, 20 nm (0.788 μin) diameter contact area of ultrasonic AFM can measure the properties of each nano-particle directly. Further research is required to compare both results via homogenization, a multi-scale modeling. Nevertheless, AFAM and nanoindentation measurements are comparable since the peak probability appears in the same range of 10 GPa (1450 ksi) to 20 GPa (2900 ksi) for both measurements.

## CONCLUSIONS

Inherent heterogeneity of cement-based materials such as the ITZ and various hydrates (C-S-H or CH) requires developing a reliable technique for materials characterization at the nanoscale. This paper reviewed two nanoscale techniques, i.e., nanoindentation and ultrasonic AFM studied at the center for ACBM and the basic principle to determine mechanical properties in both cases was discussed. Both techniques were proved to be effective in determining the local mechanical properties at the nanoscale, obtaining the comparable results for cement paste. Further research is ongoing to characterize cement-